Heat Mass Transfer (2006) 42: 492–500
DOI 10.1007/s00231-005-0046-x

SPECIAL ISSUE

C. Herman · Z. Travnicek

Cool sound: the future of refrigeration? Thermodynamic and heat transfer issues in thermoacoustic refrigeration

Received: 14 June 2004 / Accepted: 31 January 2005 / Published online: 18 November 2005

Abstract During the past two decades the thermoacoustic refrigeration and prime mover cycles gained importance in a variety of refrigeration applications. Acoustic work, sound, can be used to generate temperature differences that allow the transport of heat from a low temperature reservoir to an ambient at higher temperature, thus forming a thermoacoustic refrigeration system. The thermoacoustic energy pumping cycle can also be reversed: temperature difference imposed along the stack plates can lead to sound generation. In this situation the thermoacoustic system operates as a prime mover. Sound generated by means of this thermoacoustic energy conversion process can be utilized to drive different types of refrigeration devices that require oscillatory flow for their operation, such as thermoacoustic refrigerators, pulse tubes and Stirling engines. In order for a thermoacoustic refrigeration or prime mover system as well as a thermoacoustic prime mover driving a non-thermoacoustic refrigeration system to be competitive on the current market, it has to be optimized in order to improve its overall performance. Optimization can involve improving the performance of the entire system as well as its components. The paper addresses some of the thermodynamic and heat transfer issues relevant in improving the performance of the thermoacoustic system, such as optimization for maximum COP, maximum cooling load and the role of the heat exchangers. Results obtained using the two optimization criteria are contrasted in the paper to illustrate the complexity of the optimization process.

C. Herman (✉)
Department of Mechanical Engineering,
The Johns Hopkins University, 3400 North Charles Street,
Baltimore, MD 21218, USA
E-mail: cherman@jhu.edu

Z. Travnicek
Institute of Thermomechanics, Academy of Sciences of the Czech Republic, Prague, Czech Republic

1 Introduction

In recent years environmental issues have become a key concern in the design and development of refrigeration systems. Current research and engineering efforts focus on the development of alternative refrigerants as well as alternative technologies, such as Stirling engines, pulse-tube refrigerators, thermoelectric refrigerators, etc., which can reduce the need for hazardous refrigerants [1]. One promising approach in the class of alternative technologies is thermoacoustic refrigeration [1–5]. Thermoacoustic refrigeration was developed during the past two decades as a new, environmentally safe refrigeration technology [6–8]. The operation of thermoacoustic refrigerators employs acoustic power to pump heat.

The rapid advances in thermoacoustic theory and modeling as well as hardware development are promising, and the expectation is that thermoacoustics will become commercially viable in the near future. Thermoacoustic refrigeration is attractive from an environmental perspective because it does not rely on hazardous refrigerants. Although nowadays thermoacoustic refrigerators can achieve a substantial fraction of Carnot's efficiency (COPR = 0.1–0.2 contrasted to 0.33–0.5 for conventional refrigeration) [9], they are not yet competitive to commercial refrigerators whose operation is typically based on the Rankine cycle [1]. The basic physics and thermodynamics underlying thermoacoustic processes are already well understood [6–7, 9–14]. As a consequence, the next step in developing efficient devices is to apply sophisticated engineering tools to improve and optimize their design and performance.

2 Thermoacoustic heat pumping in a refrigerator

The thermodynamic cycle of the thermoacoustic refrigerator (TAR) relies on the Brayton cycle, which, in terms of thermodynamic performance, needs to be contrasted

to the Rankine cycle in a conventional vapor compression system. The thermoacoustic heat pumping cycle is discussed in more detail in this section, and a simple Lagrangian approach is used to visualize the physical processes responsible for the pumping of heat from the low temperature reservoir to the ambient at a higher temperature.

The schematic of a thermoacoustic refrigerator is shown in the bottom portion of Fig. 1a. Using an acoustic driver, the working fluid in the resonance tube is excited to generate an acoustic standing wave. In the design in Fig. 1a, the length of the resonance tube corresponds to half the wavelength of the standing wave, $\lambda/2$. Other resonator lengths are also possible. The pressure and velocity distributions in the resonance tube are indicated in Fig. 1b. When introducing a densely spaced stack of plates of length Δx at a location specified by the stack center position x_c into the acoustic field, a temperature difference ΔT develops along the stack plates. This temperature difference is caused by the thermoacoustic effect, and the region in which it develops is the thermoacoustic core, which includes stack plates and the working fluid between the stack plates [9] in the analysis presented in this paper. The temperature distribution along the resonance tube is shown in Fig. 1c.

A closer look into the thermoacoustic core (magnified region in Fig. 1a) reveals the mechanism responsible for thermoacoustic heat pumping by considering the oscillation of a single gas parcel of the working fluid along a stack plate. The gas parcel is at a temperature T when the cycle begins. In the first step the gas parcel moves to the left (towards the pressure antinode) and this movement is induced by the acoustic standing wave. During this process the gas parcel is subjected to adiabatic compression, which causes its temperature to rise by two arbitrary units, to reach the temperature T^{++}. In this state the gas parcel is warmer than the stack plate, which results in irreversible heat flow from the gas parcel towards the stack plate. The temperature of the gas parcel after this step is T^{+}. On its way back to the initial location the gas parcel experiences adiabatic expansion and cools down by two arbitrary units, to reach the temperature T^{-}. Now that the gas parcel is colder than the stack plate, heat flows from the stack plate towards the gas parcel and the heat transfer process is irreversible. After these steps the gas parcel has completed one thermodynamic cycle, it has reached its initial location and temperature T, and therefore the cycle can start again.

Since there are numerous gas parcels oscillating in the thermal boundary layer region along the stack plate, which are subjected to this thermodynamic cycle, heat that is deposited on the plate by one gas parcel is transported further by the adjacent parcel. This large scale heat transport process is illustrated in the bottom portion of the magnified region of Fig. 1a, showing the overall temperature gradient that develops along the stack plates.

The described cycle can also be reversed by imposing a temperature gradient ΔT along the stack plates. In this situation the directions of irreversible heat transfer and work flux are reversed, and the thermoacoustic device will operate as a prime mover, also known as the thermoacoustic engine in the thermoacoustic literature.

In order to exploit the thermoacoustic effect for heat pumping purposes, heat exchangers are attached at both ends of the thermoacoustic core. The cold heat exchanger removes heat from the low temperature reservoir (directly or by means of a coolant circulating between the refrigerated volume and the heat exchanger) at temperature T_r and supplies it to the cold side of the thermoacoustic core at the temperature T_c. The role of the hot heat exchanger, operating at temperature T_h, is to reject the heat pumped along the thermoacoustic core together with the absorbed acoustic work to the environment, which is at a higher temperature T_e. Again a coolant circulating between the ambient and the hot heat exchanger may be used.

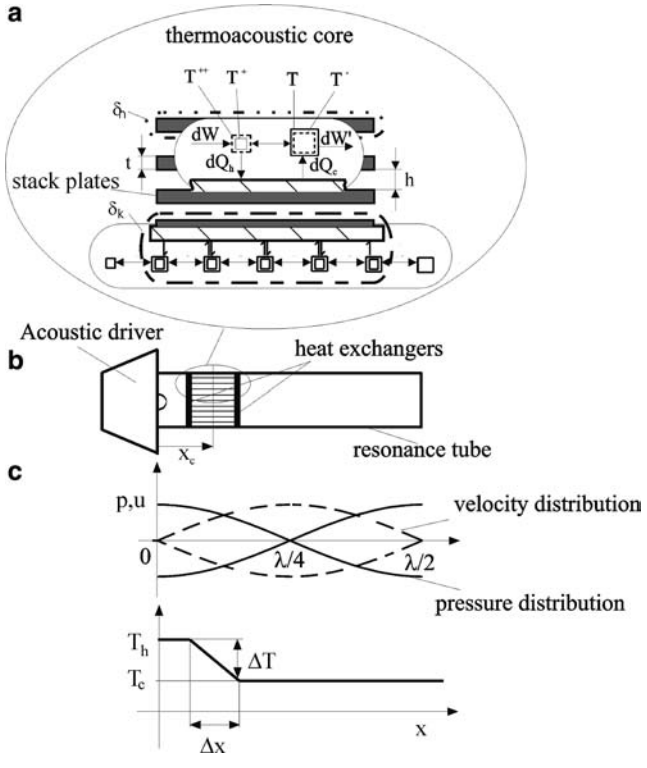

Fig. 1 **a** Schematic of the thermoacoustic refrigerator and the heat pumping process (in the magnified region). **b** Pressure, velocity and **c** temperature distributions in the resonance tube

3 Design optimization of thermoacoustic refrigerators

In mathematical sense optimization involves determining the maximum or the minimum of a function of one or more variables. In engineering optimization an optimization criterion is selected depending on the application and design goals: it may involve a range of practical

and economic criteria in addition to the thermodynamic criteria. The optimization criterion is then formulated in mathematical form, as a function (objective function). The relevant physical parameters determining the performance of the thermoacoustic system considered in the paper form the parameter space for the optimization process. The maximum or minimum of the objective function is then determined for a range of parameters of practical importance. In the design optimization of thermoacoustic refrigerators two optimization criteria were considered. One goal of the optimization was to achieve the highest COP for a particular system configuration and set of operating conditions. This is a common criterion used to compare the performance of refrigeration systems and it is useful when designing larger thermoacoustic systems. For small-scale thermoacoustic systems the cooling load Q_{load} was found to be critical for the success of the design, and therefore the design objective was to achieve the maximum cooling load.

3.1 Optimization for the best coefficient of performance

A systematic design methodology for thermoacoustic refrigerators based on a first law analysis of the thermoacoustic refrigerator viewed as a thermodynamic system was introduced by Wetzel and Herman [9]. In a thermodynamic analysis the coefficient of performance, COP, defined as

$$\text{COP} \equiv \frac{\text{heat extracted at lower temperature } T_{\text{r}}}{\text{work done on the machine}} \equiv \frac{Q_{\text{load}}}{E_{\text{el}}}, \tag{1}$$

is typically used to describe the overall thermodynamic performance of refrigerators. The second law of thermodynamics limits the value of COP as $\text{COP} \leq \text{COP}_{\text{C}}$, where Carnot's coefficient of performance is the COP of the ideal Carnot cycle defined as

$$\text{COP}_{\text{c}} = T_{\text{c}}/(T_{\text{h}} - T_{\text{c}}) \tag{2}$$

T_{h} and T_{c} are the temperatures of the hot and cold heat exchangers in a thermoacoustic refrigerator, respectively. The TAR has to be designed in such a way that the intrinsic irreversibilities associated with the heat transfer in the system are encouraged.

The energy conversion processes in the components of the thermoacoustic refrigerator system are illustrated in the energy flow diagram in Fig. 2. Two main energy flows can be identified in Fig. 2. Energy transformations along the vertical axis indicate energy conversion steps from the electrical energy E_{el} being added to the thermodynamic system, converted into work W_{tot} (in the form of acoustic energy—sound) and then delivered to the components of the thermoacoustic refrigerator. A portion of the acoustic work W_{dis} is dissipated in the resonance tube and heat exchangers. These losses are discussed in detail in Ref. [9]. The remaining portion of the acoustic work W_{tc} is used to drive the thermoacoustic heat flow process. The heat flow from the low temperature reservoir to the ambient at a higher temperature is illustrated along the horizontal axis in Fig. 2. Losses of acoustic power at the different components of the refrigerator are added to this heat flow.

The electric power introduced into the system E_{el}, is converted into work, i.e. acoustic power W_{tot}, in the acoustic driver. The electroacoustic conversion efficiency η_{elac} is defined as

$$\eta_{\text{elac}} \equiv \frac{W_{\text{tot}}}{E_{\text{el}}} = \frac{W_{\text{tc}} + W_{\text{dis}}}{E_{\text{el}}} = \frac{W_{\text{tc}} + W_{\text{res}} + W_{\text{ex}}}{E_{\text{el}}}. \tag{3}$$

η_{elac} is of the order of 3% for commercial loudspeakers. Efficiencies of 50% were demonstrated in dedicated drivers and values up to 90% should be possible [9].

The thermodynamic analysis of Wetzel and Herman [9] showed that for optimization purposes the thermoacoustic refrigerator is best subdivided into four main modules: (1) thermoacoustic core, (2) resonance tube, (3) heat exchangers and (4) acoustic driver. This modular description is suitable for design purposes as it allows the designer to optimize each module separately, and obtain a global thermodynamic performance maximum of the thermoacoustic refrigerator as a result.

Equation 3 suggests that not all of the converted acoustic power W_{tot} can be exploited to pump heat through the thermoacoustic core. The thermoacoustic effect occurs not only within the thermoacoustic core, where it is responsible for the pumping of heat, as described by the component W_{tc} in Eq. 3. Simultaneously, it occurs on surfaces of the resonance tube and the heat exchangers, where its contribution is dissipative, W_{dis} (Eq. 3). These two components, W_{tc} and W_{dis}, comprising the total acoustic power W_{tot}, are shown in Fig. 2. The acoustic power losses within the hot portion of the resonance tube and at the hot heat exchanger (included in the terms W_{res} and W_{ex} in Eq. 3 and shown as W_{hres} and W_{hex} in Fig. 2, respectively) act as additional heating loads on the hot heat exchangers. The acoustic power losses in the cold portion of the resonance tube and at the cold heat exchanger (shown as W_{cres} and W_{cex} in Fig. 2, respectively) act as additional cooling loads on the cold heat exchanger.

Considering the energy flows in Fig. 2 and keeping in mind the fact that the thermoacoustic heat pumping takes place within the thermoacoustic core, the upper limit of the thermoacoustic refrigerator's thermodynamic performance is determined by the performance of the thermoacoustic core, defined as

$$\text{COP}_{\text{tc}} \equiv \frac{\text{heat extracted at lower temperature } T_{\text{c}}}{\text{work done on the thermoacoustic core}} \equiv \frac{Q_{\text{c}}}{W_{\text{tc}}}. \tag{4}$$

The analysis of Wetzel and Herman [9] indicates that the COP_{tc} can be estimated applying a simplified linear

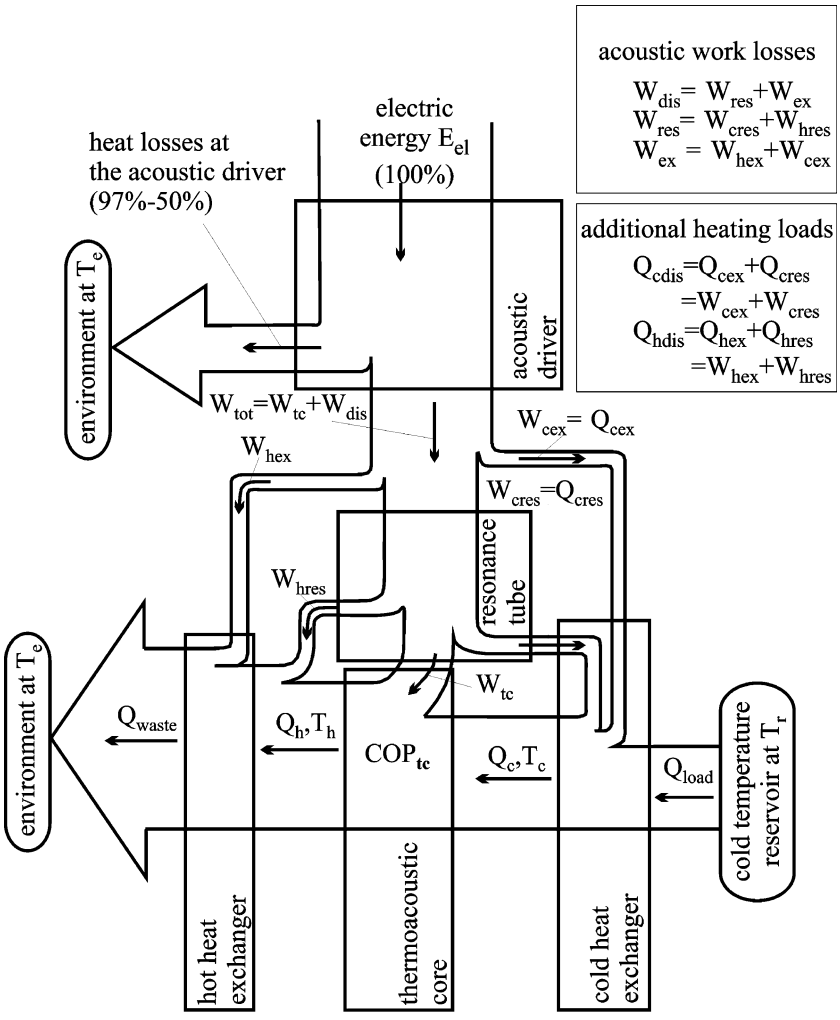

Fig. 2 Energy flows in a thermoacoustic refrigerator [9]

model of thermoacoustic processes, the short stack boundary layer approximation [7].

The critical, least understood and studied components of thermoacoustic refrigerators are the two heat exchangers. Their manufacturing is difficult and expensive, and past solutions were often limited by manufacturing considerations rather than based on the optimization of their thermal performance. In some cases heat exchangers can cause substantial flow blockage in the resonance tube accompanied by a large pressure drop penalty. This pressure drop is another mechanism that contributes to the dissipation of acoustic power on the heat exchangers. The difficulty of modeling thermoacoustic heat transfer in the heat exchangers is that the flow is oscillatory with zero mean velocity. In such situations, standard heat exchanger design methods, such as the effectiveness, number of transfer units (NTU) method or the logarithmic mean temperature difference (LMTD) method, developed for steady flow, cannot be applied directly. The effectiveness ε of the cold heat exchanger is defined similar to that in conventional heat exchanger analysis [19] as ε = heat transferred/maximum heat transferable = $Q_{load}/Q_c = 1 - Q_{cdis}/Q_c = 1 - (Q_{cres}+Q_{cex})/Q_c$.

This definition reflects the fact the heat transfer in the cold heat exchanger is limited by the amount of heat the thermoacoustic core is capable of absorbing at the low temperature T_c. Therefore the maximum heat transferable corresponds to Q_c. However, $Q_{load} < Q_c$ because of the dissipation of acoustic power, and the transferred heat (removed from the low temperature reservoir) is limited to the cooling load Q_{load}.

Combining Eqs. 1, 2, 3, 4 yields an expression for the overall COP of a thermoacoustic refrigerator

$$\mathrm{COP} = \eta_{elac}\varepsilon\frac{W_{tc}}{W_{tot}}\frac{Q_c}{W_{tc}} = \eta_{elac}\,\varepsilon\,\eta_{ac}\,\mathrm{COP}_{tc}. \quad (5)$$

The acoustic power efficiency term $\eta_{ac} \equiv W_{tc}/W_{tot}$ in Eq. 5 accounts for the fact that not all of the converted acoustic power W_{tot} can be used to pump heat through the thermoacoustic core. η_{ac} achieves its maximum value of one when there is no acoustic power dissipation, $W_{dis} = 0$, in the heat exchangers and in the resonance tube. It follows from the basic definitions that the maximum possible values for the electroacoustic efficiency η_{elac} and the effectiveness ε of the cold heat exchanger are also one. Therefore, the overall COP of the

thermoacoustic refrigeration system reaches its maximum value, corresponding to the COP_{tc} of the thermoacoustic core, when the two efficiencies, η_{elac} and η_{ac}, as well as the effectiveness ε reach their maximum value of one. This is the situation considered in the optimization algorithm developed by Wetzel and Herman [9]. The assumption is that the four terms of Eq. 5, η_{elac}, ε, η_{ac} and COP_{tc} are independent. This assumption certainly holds for η_{elac}. Since the COP_{tc} for some design solutions may depend on the design of the resonance tube and the heat exchangers, interdependence of COP_{tc}, ε and η_{ac} needs to be considered in a more detailed and advanced optimization procedures. However, the optimization method discussed here already yields very good data for design purposes.

3.1.1 Parameter spaces

The first step in the optimization algorithm introduced by Wetzel and Herman [9] is the design and optimization of the thermoacoustic core. The design begins by establishing the design requirements for a specific device, depending on the application. The basic design requirements for a thermoacoustic refrigerator are twofold: (1) the refrigerator has to supply the desired cooling load (Q_{load} in Fig. 2) and at the same time (2) it has to achieve the prescribed cooling temperature (T_r in Fig. 2). The result of the short stack boundary layer approximation yields two equations describing the enthalpy flux H and work flux W. These equations were originally derived by Rott [14] and developed further by Swift [7]. The enthalpy and work fluxes are needed to estimate the COP of the thermoacoustic core as

$$COP_{tc} = \frac{|H| - |W|}{|W|} = \frac{Q_c}{W_{tc}}. \tag{6}$$

An examination of the equations describing the heat and work fluxes (details available in Ref. [9] and will not be repeated here) suggests that the COP_{tc} is dependent on a large number of parameters: geometrical, such as stack length Δx, half the plate spacing y_0; parameters of the working fluid, such as the density and the Prandtl number ρ_m and σ; sound wave characteristics and geometry, angular frequency ω; operating parameters, such as mean pressure p_m, etc. 19 independent design parameters were initially identified in these equations, and they were organized systematically by introducing the multidimensional parameter space shown in Table 1. The multidimensional parameter space is divided into three subspaces: (1) the design requirements specifying the operational requirements of the thermoacoustic core, (2) the material specific design parameters describing the thermophysical properties of the working fluid and the stack plates and (3) the geometry specific design parameters, which are shown in Fig. 1. The enthalpy flux is proportional to the factor $T_m\beta$. Considering only ideal gases or liquids close to their critical point (for which $T_m\beta = 1$) as potential working fluids, as suggested by Swift [7], the thermal expansion coefficient β can be omitted from the list of material specific design parameters. In this way, the number of independent design parameters is reduced to 18.

In Fig. 3 the results of performance calculations, illustrating the efficiency of the thermoacoustic core, are shown. They are presented in terms of the $COPR_{tc}$ as function of the normalized stack length ξ. Presenting the results of the performance calculations in form of the COPR rather than the COP offers the advantage that the trivial Carnot part of the performance, accounting for the temperature dependence of the efficiency, is eliminated. Wetzel and Herman [9] combined the terms of the multidimensional parameter space into dimensionless groups and reduced the number of key design parameters to 6. In terms of the normalized design parameters, the $COPR_{tc}$ can be determined as

$$COPR_{tc} = \frac{COP_{tc}}{COP_C} = \frac{(|\Phi_H| - |\Phi_W|)/|\Phi_W|}{(2-\theta)/(2\theta)} \tag{7}$$

In Eq. 7, θ is the normalized temperature difference defined as $\theta \equiv \frac{\Delta T}{T_m} = \frac{T_h - T_c}{T_m}$, with T_m being the mean temperature of the working fluid. Φ_H and Φ_W are the normalized work and enthalpy fluxes [9]. In Fig. 3a the influence of the working fluid on the coefficient of performance of the thermoacoustic core is illustrated. The parameter for the curves is the Prandl number σ of the working fluid. Suitable working fluids for thermoacoustic refrigerators are noble gases. The Prandtl number is $\sigma = 0.67$ for all noble gases [20]. In order to lower the Prandtl number, noble gases are mixed to form a more suitable combination for thermoacoustic applications.

Table 1 Multidimensional parameter space describing the design parameters of the thermoacoustic core [9]

Design requirements	Material specific parameters	Geometry specific parameters
Q_c, cooling load of the thermoacoustic core	Working fluid	Δx, stack length
$(\|H\|-\|W\|) > Q_{load}$	K, thermal conductivity	x_c, stack center position
ΔT, desired temperature span	a, speed of sound	$h = 2y_0$-plate spacing
T_m, mean operating temperature	μ, dynamic viscosity	$t = 2l$-plate thickness
p_m, mean pressure	γ, ratio of specific heats, c_p/c_v	A, cross-sectional area
P_A, peak pressure amplitude	β, thermal expansion coeff.	
f, resonant frequency	Stack material ρ_s, mean density	
	c_s, specific heat K_s, thermal conductivity	

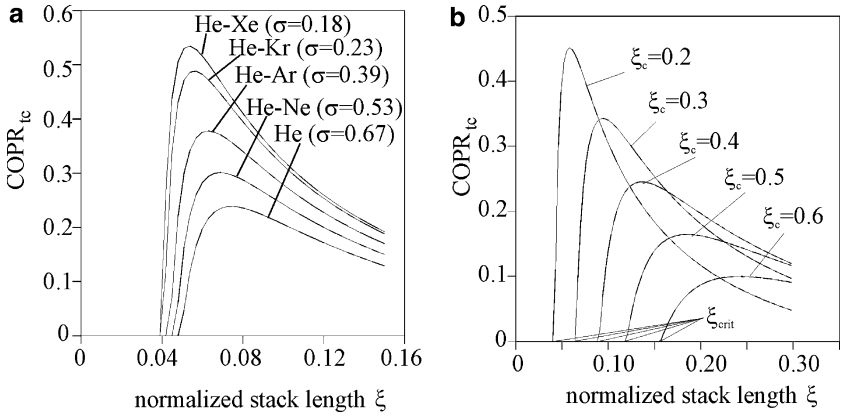

Fig. 3 Performance of the thermoacoustic core in terms of the $COPR_{tc}$ as function of the normalized stack length $\xi = 2\pi\Delta x/\lambda$, with λ being the wavelength of the sound wave: **a** for five woking fluids [He–Xe(62%/38%), He–Kr(60%/40%), He–Ar(58%/42%) and He–Ne(55%/45%) and pure He] as well as **b** for different stack center positions

The Prandtl numbers σ for the different noble gas mixtures are shown in Fig. 3 [He–Xe(62%/38%), He–Kr(60%/40%), He–Ar(58%/42%), He–Ne(55%/45%) and pure He]. The results of these calculations agree well with the expectations. Decreasing the Prandtl number σ increases the difference between the thermal and viscous penetration depths and therefore more working fluid contributes to the thermoacoustic effect, which leads to an increase in the efficiency of the thermoacoustic core. By choosing the He–Xe mixture as a working fluid instead of pure Helium, the $COPR_{tc}$ can be increased approximately by a factor of two.

In Fig. 3b results that quantify the effect of the stack center position on the $COPR_{tc}$ are displayed. For this purpose, the normalized stack length ξ was optimized and the normalized stack center position ξ_c was varied as a parameter. The rest of the normalized design parameters remained the same, and more details regarding the application and numerical values can be found in Ref. [9]. The results suggest that by placing the stack closer to the pressure antinode, which means decreasing the normalized stack center position ξ_c, the $COPR_{tc}$ increases. This can be explained by the fact that higher pressure amplitudes at the pressure antinode cause more pronounced temperature changes. It can also be observed that as the normalized stack center position ξ_c decreases, the optimum normalized stack length ξ_{opt} becomes increasingly shorter. When inspecting the optimum normalized stack length ξ_{opt} and the normalized critical stack center position ξ_{crit} in Fig. 3b, one would suspect that these two parameters are somehow related. Indeed, that is the case.

The results suggest that there is a distinct optimum of the coefficient of performance for a selected set of operating conditions. The optimum design in this case specifies the geometrical characteristics of the thermoacoustic core. In order to achieve high COPs, a low Prandtl number working fluid (combination on noble gases) is the best choice.

3.2 Optimization for maximum cooling load

The first law of thermodynamics yields an expression for the cooling load of the thermoacoustic core in the form

$$Q_C = A\, p_m\, a\, (\Phi_H - \Phi_W), \tag{8}$$

In Eq. 8 A is the cross-sectional area of the resonance tube, p_m the mean pressure of the working fluid and a the speed of sound. Taking into account that the sound speed in an ideal gas a (which depends on the thermophysical properties of the fluid) scales with $T_m^{0.5}$, and the cross-sectional area of the TAR scales with the diameter of the resonance tube D as D^2, the cooling load can be expressed as

$$\begin{aligned} Q_C &= (\pi/4)\, D^2\, p_m\, DR^2\, T_m^{0.5} \\ &= F(\sigma,\ \gamma,\ \varepsilon_s,\ \theta,\ \xi,\ \xi_C,\ BR,\ \delta_{kh}), \end{aligned} \tag{9}$$

where the function $F(\sigma, \gamma, \varepsilon_s, \theta, \xi, \xi_C, BR, \delta_{kh})$ depends on eight non-dimensional parameters (their detailed description is available in Ref. [9]). The parameters of the function F in Eq. 9 are summarized in Tables 2 and 3 for the hardware design and seven working fluids specified in these tables. The influence of individual parameters on the TAR performance, in particular on the Q_C, is evaluated using Eq. 9. Although this influence was considered by Swift [7] in a general sense, and recently by Wetzel and Herman [9] by considering the COP and COPR as the performance criterion, a further systematic study of the influence of system parameters is necessary. This is especially important when optimizing TARs to be used for the cooling of electronic components, where the main objective is to achieve high cooling loads. The cooling load is more important than the COP in this situation.

3.2.1 *Effect of the working fluid*

Table. 2 and 3 summarize some of the design and calculated parameters associated with the selected working fluids, such as sound speed and thermal penetration depth. It is worth noting that the stack plate thickness and spacing depend on the thermal penetration depth, thus also on the choice of the working fluid, and they are included in Table. 2 and 3. Conversely, the non-dimensional parameters blockage ratio, BR, and δ_{kh} are the same for all discussed working fluids (BR = 0.80 and $\delta_{kh} = 0.46$). Since the working fluid is varied in these calculations, the heat capacity correction factor ε_s

Table 2 Design parameters

Design requirements		
Mean pressure	p_m [Pa]	500,000
Drive ratio	DR [%]	3.5
Cold side temperature	T_C [K]	323.15
Hot side temperature	T_H [K]	333.15
Mean operating temperature	T_m [K]	328.15
Non-dimensional temperature diff.	θ	0.030
Carnot's coeff. of performance	COP_c	32.32
Stack material	Mylar	
Geometry specific parameters		
Resonator length	$L = 21.3$ mm	
Thermoacoustic core diameter	$D = 10.2$ mm	
Relative free cross section	BR = 0.80	
Inverse normalized plate spacing	$\delta_{kh} = 0.460$	

changes as well, and is in the range of 0.024 (air) $< \varepsilon_s <$ 0.048 (pure He) (last row of Table 3).

The influence of the working fluid on the TAR cooling load is exerted through the parameters σ, γ, and ε_s, as described by Eq. 9. Figure 4a shows results of performance calculations in terms of the COPR for the seven working fluids whose properties are summarized in Table 3. A similar result was discussed by Wetzel and Herman [9]. All plotted curves were calculated for the same characteristic temperatures $T_C = 323.15$ K, $T_H = 333.15$ *K*, i.e. at $COP_C = 32.3$ (Table 2); the curves differ only in terms of the working fluid used. The comparisons in the present study are made for different noble gases and their mixtures as well as for air. All curves in Fig. 4 were calculated for the normalized stack center position $\xi_C = 0.49$. This choice of ξ_C is a result of TAR optimization for Helium as working fluid (as in Fig. 5b).

According to the expectations, the smallest COPR-values are obtained for air as working fluid, which suggests that there are no thermodynamic reasons for using air in TAR design for practical applications. A calculation for air was performed mainly for comparison purposes (and because of the wide availability of air as well as the simplicity of its use). In Fig. 4a the curve for air is shifted towards the higher values of ξ, because of smaller the c_p/c_v values for air ($\gamma = 1.4$, Table 3).

Figure 4b, c illustrate the influence of working fluids on the cooling load in non-dimensional and dimensional forms, respectively. The fixed parameters are the same as discussed for Fig. 4a (Table 2). The influence of the Prandtl number on the non-dimensional cooling load Φ_C is similar as on the COPR, i.e. the decrease of σ causes an increase of the Φ_C. However, the Φ_C–σ dependence is not as strong as the COPR–σ dependence. On the other hand, the Q_C–σ relationship displayed in Fig. 4c is quite different and the Q_C values vary in a very wide range. Helium yields the highest cooling load because Q_C scales with the speed of sound ($= 1054.4$ m/s and the corresponding thermophysical properties, Table 3). In contrast with the COPR–σ relationship in Fig. 4a, small values of the Prandtl number do not necessarily yield a high cooling load. For example, despite of the fact that the Prandtl number of the He–Xe 62%–38% gas mixture is very small (the smallest of all, $\sigma = 0.18$, curve 7), it yields relatively small cooling load, the maximum of which is comparable to that of air (curve 1). The cooling load with Helium as working fluid (curve 2) is nearly three times higher. A TAR with Helium as the working fluid can be considered as the limiting case of the most powerful TAR; it delivers the highest cooling load of all noble gases and their mixtures examined in the present study. Helium is suggested for design of TAR for electronic cooling applications, therefore the curve for Helium is highlighted by thicker line; the maximum of this curve is recommended as the operating point of the device.

It is worth noting that the effect of working fluid on the TAR performance can be very important for a small

Table 3 Legend of curves

Curve		1	2	3	4	5	6	7
Working fluid		Air	He	He–Ne 55–45%	He–Ar 58–42%	He–Xe 89–11%	He–Kr 60–40%	He–Xe 62–38%
Prandtl number	σ	0.71	0.67	0.53	0.39	0.27	0.23	0.18
Ratio c_p/c_v	γ	1.40	1.63	1.64	1.65	1.67	1.65	1.64
Calculated parameters								
Sound speed	a [m/s]	362.9	1054.4	628.9	485.0	500.6	353.6	292.4
Resonant frequency, c/λ	f [Hz]	8,519	24,752	14,763	11,384	11,751	8,300	6,864
Thermal penetration depth	δ_κ [mm]	0.014	0.023	0.022	0.021	0.027	0.024	0.024
Plate spacing, ($h = \delta_\kappa/\delta_{\kappa h}$)	h [mm]	0.030	0.049	0.048	0.045	0.058	0.051	0.052
Plate thickness, [$= h$(1-BR)/BR]	t [mm]	0.008	0.012	0.012	0.011	0.014	0.013	0.013
Heat correction factor	ε_S	0.024	0.048	0.036	0.030	0.039	0.030	0.027

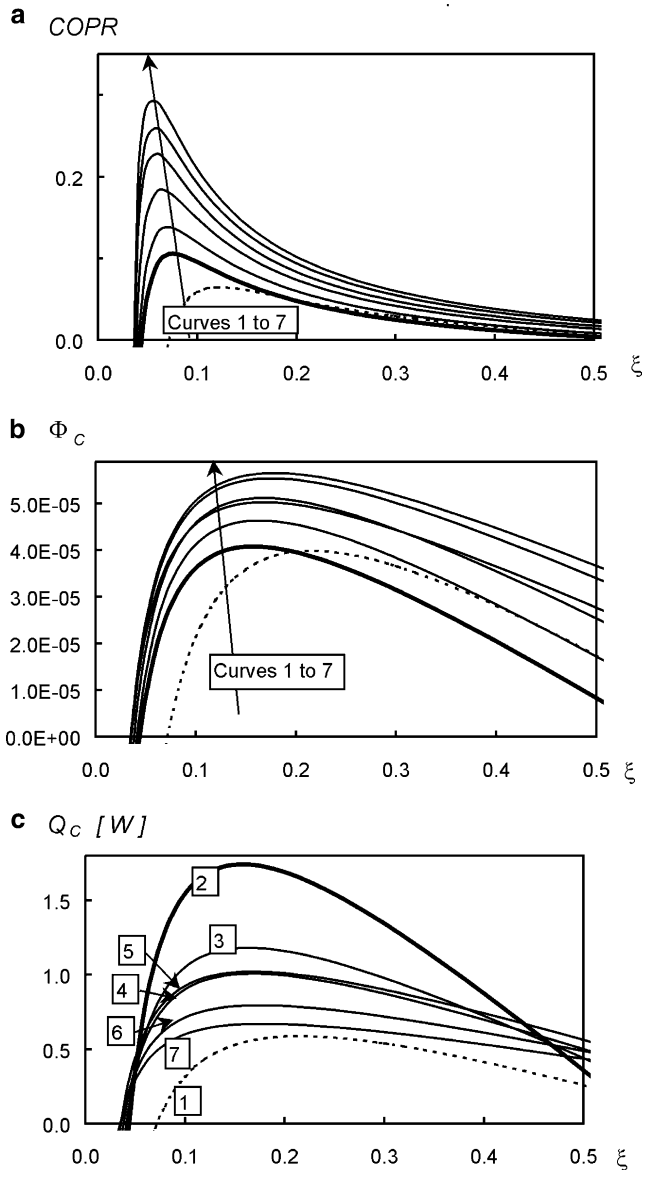

Fig. 4 **a** COPR and cooling load in **b** non-dimensional and **c** dimensional form as function of the dimensionless stack length ξ for the seven working fluids specified in Table 3

device, such as the design for the cooling of electronics considered in the present study. Choosing a short resonance tube increases the acoustic frequency ($f \sim L^{-1}$) and decreases the thermal penetration depth ($\delta_\kappa \sim f^{-1/2}$, thus $\delta_\kappa \sim L^{1/2}$). The stack plate spacing h is proportional to the thermal penetration depth, $h \sim \delta_\kappa \sim L^{1/2}$. The small dimensions of stack plates (t, h) desirable in thermoacoustic applications could be a source of manufacturing problems. The present choice of the working fluid for electronic cooling applications is Helium, which yields a stack plate thickness $t = 0.012$ mm.

Table 3 shows the resonant frequency for the working fluids considered. The present resonator length is relatively short (21.3 mm), therefore resonant frequencies are high. The frequency is highest for Helium, because of the high sound speed in He. It should be noted that the designers have to take into account possible operating problems associated with Helium as the working fluid, such as the well-known leakage and diffusion through solid walls.

The input parameters for the TAR design (or sizing) problem are the thermophysical parameters, the temperatures T_H and T_C, mean pressure and drive ratio, material specific parameters and geometry constraints. 2D-graphs with contour lines representing constant values of COPR and Q_C/Q_{CMAX}, respectively, where Q_{CMAX} is the local maximum of the cooling load ($=1.74$ W) are presented in Fig. 5. Figure 5a shows that the region of stack lengths and stack center positions ξ_C, ξ characterized by favorable operation of the TAR (using COPR as optimization criterion) is localized in a relatively small portion of the $\xi_C - \xi$ plane. The results suggest that for an arbitrarily chosen fixed value of ξ_C a maximum value of the COPR can be found as a function of ξ. For an arbitrarily chosen, fixed value of ξ a maximum of the COPR can be found as a function of ξ_C.

The maximum of the function COPR(ξ_C, ξ) is relatively close to the origin of the coordinate system, but not in the origin itself ($COPR_{MAX} = 0.38$ for $\xi_C = 0.05$ and $\xi = 0.005$). As shown in Fig. 5b, the maximum of the function $Q_C(\xi_C, \xi)$ is located far away from the origin of the coordinate system. For the results in Fig. 5b, i.e. for Helium and the parameters from Tables 2 and 3, this maximum is located at $(\xi_C = 0.49,\ \xi = 0.16)_{OPT.}$ The TAR optimization for electronic cooling applications (small refrigerator) is based on the Q_C maximization, therefore these coordinates represent the optimum solution to the design problem for a particular working fluid.

A comparison of Fig. 5a, b leads to the conclusion that the maxima of the functions COPR(ξ_C, ξ) and $Q_C(\xi_C, \xi)$ do not coincide; the former is located relatively close to the to the origin of the coordinate system, the latter is far away from that point. However, under specific operating conditions of the TAR, in some applications increasing of the COPR can be desirable, thus the operating point of the TAR can be moved towards COPR maximum. A practical design of the TAR can require for its operating point to be between the maxima of the COPR(ξ_C, ξ) and the $Q_C(\xi_C, \xi)$. However, this compromise is not supported by any direct optimization criterion (rather it uses an objective function that combines two direct thermodynamic criteria and possibly some practical requirements) and is therefore not discussed here.

4 Conclusions

In this paper a systematic design approach is discussed that provides fast engineering estimates for initial design calculations of thermoacoustic refrigerators. Their performance was evaluated using two criteria. The

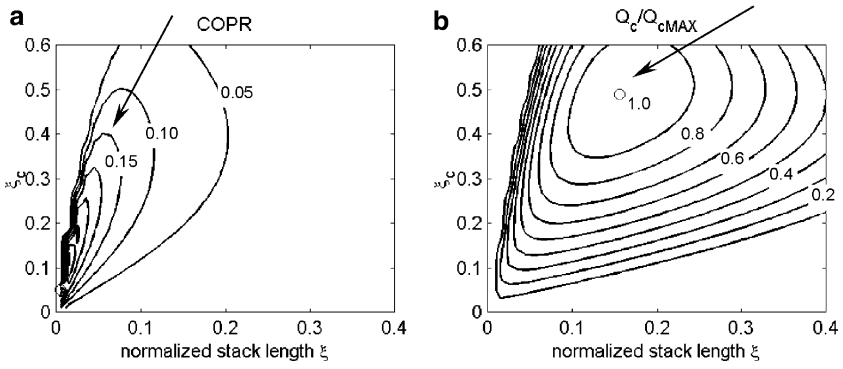

Fig. 5 Family of curves showing the dimensionless stack center position ξ_C as a function of the stack length ξ for constant values of the **a** COPR and **b** the ratio Q_C/Q_{CMAX}

methodology is based on a first law analysis that suggests a separate optimization of the four main modules of a thermoacoustic refrigerator: (1) thermoacoustic core, (2) resonance tube, (3) heat exchangers and (4) acoustic driver. An upper limit on the thermoacoustic refrigerator's performance is set by the heat pumping capacity of the thermoacoustic core. The short stack boundary layer approximation was applied to evaluate and optimize the performance of the thermoacoustic core. This simplified linear model of thermoacoustic theory was not directly suitable for design and optimization purposes in its original form. Calculations of the thermoacoustic core's performance indicate that thermoacoustic refrigeration can achieve COPRs competitive to commercially available refrigerators. Of course, when comparing data with other refrigeration systems, we have to keep in mind that the presented calculations do not include energy losses in the other three modules (resonance tube, heat exchangers and acoustic drivers) of a thermoacoustic refrigerator.

For miniature thermoacoustic refrigerators the cooling load performance is critical. The influence of working fluids on the cooling load was discussed and analyzed systematically. It is known that TARs with noble gases and their mixtures as working fluids can achieve high value of the coefficient of performance because of the small Prandtl number values. The present study reveals and quantifies that the cooling load behavior is different: the highest cooling load can be achieved with pure Helium as working fluid. A reason for this is the high sound speed in Helium. A TAR with Helium as working fluid gives the highest cooling load of all noble gases and their mixtures examined in the present study. Therefore, it is recommended as the limiting case of the TAR in terms of cooling performance (power).

Acknowledgements This work was supported by the Office of Naval Research, the Rockwell Science Corporation and DARPA. The contribution of Martin Wetzel in the development of the design optimization methods is gratefully acknowledged. The first author thanks Jeff DeNatale and C.-L. Chen for the motivating discussions regarding the cooling of electronic chips. Partial support to Z. Travnicek during the finalization of the paper, provided by the Grant Agency CR (project No. 101/05/2681), is also acknowledged.

References

1. Gauger DC, Shapiro HN, Pate MB (1995) Alternative technologies for refrigeration and air-conditioning applications, Environmental Protection Agency Publication EPA/600/SR-95/066
2. Wheatley JC, Hofler T, Swift GW, Migliori AJ (1983) An intrinsically irreversible thermoacoustic heat engine. J Acoust Soc Am 74(1):153–170
3. Wheatley J, Hofler T, Swift GW, Migliori A (1985) Understanding some simple phenomena in thermoacoustics with applications to acoustical heat engines. Am J Phys 53(2):147–161
4. Wheatley JC, Swift GW, Migliori A (1986) The Natural Heat Engine, Los Alamos Science, No. 14, Fall 1986
5. Swift GW (1995) Thermoacoustic engines and refrigerators, Physics Today, July 1995, pp. 22–28
6. Wheatley JC (1986) Intrinsically irreversible or natural engines, Los Alamos National Laboratory—MS K764
7. Swift GW (1988) Thermoacoustic engines. J Acoust Soc Am 84(4):1145–1180
8. Hofler TJ (1986) Thermoacoustic refrigerator design and performance. Dissertation, University of California, San Diego
9. Wetzel M, Herman C (1997) Design optimization of thermoacoustic refrigerators. Int J Refrig 20(1):3–21
10. Worlikar A, Knio O (1996) Numerical simulation of a thermoacoustic refrigerator. J Comp Phys 127:424–451
11. Atchley AA, Hofler TJ, Muzzerall ML, Kite D, Ao CD (1990) Acoustically generated temperature gradients in short plates. J Acoust Soc Am 88(1):251–263
12. Wetzel M, Herman C (2000) Experimental study of thermoacoustic effects on a single stack plate—Part I: temperature fields. Heat Mass Trans 36:7–20
13. Wetzel M, Herman C (1999) Experimental study of thermoacoustic effects on a single stack plate—Part II: Heat Transfer. Heat Mass Trans 35:433–441
14. Rott N (1980) Thermoacoustics. Adv Appl Mech 20:135–175
15. Radebaugh R (1990) A reviw of pulse tube refrigeration. Adv Cryogenic Eng 35:1191
16. Swift GW (1997) Thermoacoustic natural gas liquefier, Proc. DOE Natural Gas Conference, Houston
17. Swift GW, Martin RA, Radebaugh R (1990) Acoustic cryocooler, US Patent No. 4,953,366
18. Radebaugh R, McDermott KM, Swift GW, Martin RA (1990) Development of a thermoacoustically driven orifice pulse tube refrigerator, Proc. 1990 Interagency Meeting on Cryocoolers, Plymouth, MA, (David Taylor Research Center publication DTRC-91/003, 1991)
19. Incropera FP, De Witt DP (1990) Fundamentals of heat and mass transfer. Wiley, New York
20. Giacobbe FW (1994) Estimation of Prandtl numbers in binary mixtures of helium and other noble gases. J Acoust Soc Am 96:3568–3580